이학석사학위논문

Flexible Nonvolatile Resistive Memory Devices Using Self-assembled Block Copolymer/PCBM Nanocomposites

자기 조립 블록 공중합체/PCBM 나노혼합물을 이용한 유연한 비 휘발 저항성 메모리소자 연구

2012년 8월

서울대학교대학원

나노융합학과

조 한 주

Flexible Nonvolatile Resistive Memory Devices Using Self-assembled Block Copolymer/PCBM Nanocomposites

자기 조립 블록 공중합체/PCBM 나노혼합물을 이용한 유연한 비 휘발 저항성 메모리소자 연구

지도교수 김 연 상

이 논문을 이학 석사 학위논문으로 제출함

2012년 8월

서울대학교 대학원

나노 융합학과

조 한 주

조한주의 석사학위논문을 인준함

2012년 8월

위 원 장	Jan Largerwall	(인)
부 위 원 장	김 연 상	(인)
위 원	박 원 철	(인)

Abstract

Here, the nonvolatile resistive organic memory devices based on a fullerene derivatives (PCBM) embedded in a micro-phase separated poly(styrene-*b*-methyl methacrylate) (PS-*b*-PMMA) block copolymer thin film were demonstrated. PS-*b*-PMMA diblock copolymer used in this study tends to be self-assembled into the spherical structure inside the films according to the block copolymer properties. PCBM molecules were selectively isolated in the PS nanosphere domain which resulted in well-dispersed condition of PCBM without aggregation. Controlling the aggregation of PCBM allowed the memory devices to possess the improved performance. The PS-*b*-PMMA:PCBM nanocomposite based memory devices exhibited bipolar switching phenomenon and their characteristics were continuously stable and reproducible at low operating voltages. These results make distinctions with the homopolymer:PCBM composite devices which have unstable set/reset processes and short retention time. As further application, we fabricated the flexible memory devices using PS-*b*-PMMA/PCBM nanostructure in which no significant degradation of electrical properties was observed before and after bending. By simple solution process, nonvolatile resistive memory devices which had high performance and low power consumption were successfully achieved without any additional process.

keywords: block copolymer, PCBM, ReRAM, nonvolatile memory, flexible memory

Student Number: 2010-23945

Contents

List of Figures

Figure 17. The I-V curves of the memory devices (left) and retention tests (right) (a) the device with the configuration of Al/PS containing 0.05wt% PCBM/ITO glass, (b) the device with the configuration of Al/PMMA containing 0.05wt% PCBM/ITO glass.

Figure 18. (a) A log-log plot of the current as a function of the voltage for Al/ PS_{10}-*b*-$PMMA_{130}$: PCBM (0.05wt%) /ITO glass device during the OFF state and ON state. (b) A hypothetical diagram for switching mechanism.

1. Introduction

1. 1. Organic Memory Devices

Organic memory devices have gathered a great amount of attention due to their possibility to be applied to the flexible next generation devices.[1-5] The many kinds of organic memory devices are fascinating candidates for the alternative information storage devices of current Si-based memories which have problems of scaling down in feature size and inflexibility. Polymeric materials for memory devices make possible to scale down to sub-micrometer size by using unconventional lithography methods[6, 7] and give flexibility to devices.

As shown in Figure 1, memory devices are divided into two groups: volatile and nonvolatile, and these are split into several types of memory.[8] Volatile memories such as DRAM and SRAM have a high degree of integration and a fast operation speed, but they have disadvantages that all the information is deleted after the power is turned off. To overcome this problem, nonvolatile memory which have the advantages like a high cell density, fast speed, and low power consumption are required.

For years, nonvolatile NAND and NOR type flash memories have been studied extensively as alternative memory devices and these type of devices are almost matured now.[9-11] For the next generation types of memory devices, FeRAM(Ferroelectric Random Access Memory), MRAM (Magnetic RAM), and PRAM (Phase-change RAM) are candidates currently being investigated. In addition, ReRAM(Resistive RAM) have been exploited as an emerging memory device by introducing various kinds of organic materials.

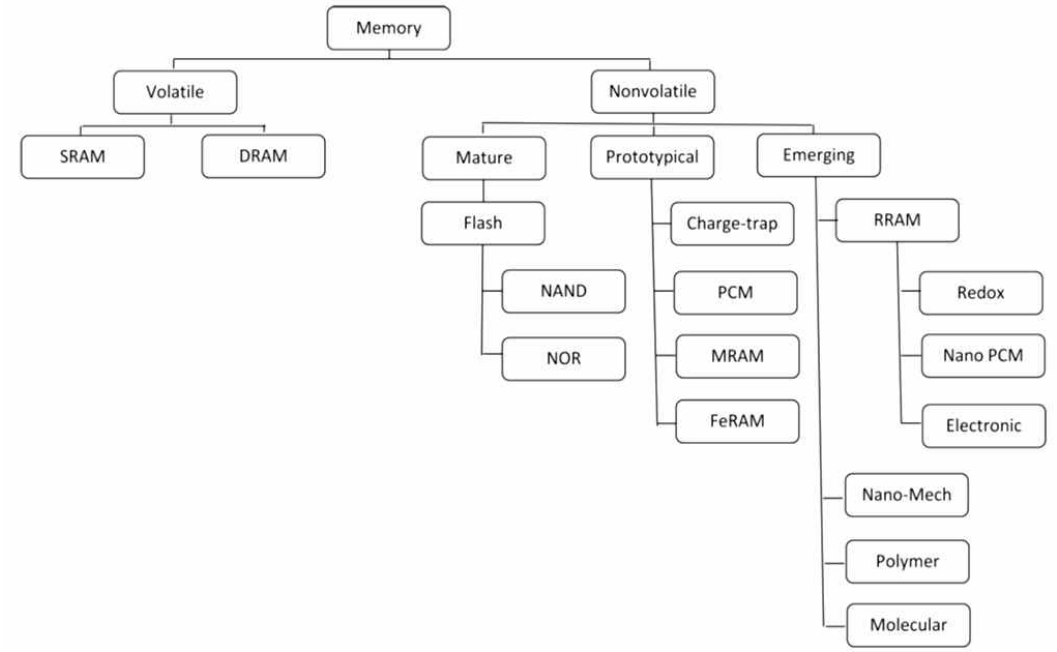

Figure 1. A diagram for the classification of memory devices.[8]

1. 2. ReRAM (Resistive Random Access Memory)

Organic ReRAM devices have many advantages such as simple structure (Metal-Insulator-Metal structure), low power consumption, high cell density, and low costs. Due to these merits, various kinds of organic materials such as a polyimide, polystyrene, and poly(methyl methacrylate) were used to fabricate the ReRAM memory devices.[12-14] To form the memory devices, the single cells should comprise electrodes and an active layer which consists of a polymeric insulating material and a charge trapping material. For the active layer, Lee *et al*. employed a synthesized polyimide with PCBM (Phenyl-C61-butyric acid methyl ester) as a charge trapping material[12, 15], Chen *et al*. introduced various kinds of block copolymers[16-18], and Kim *et al*. used poly(methyl methacrylate) with Ag or quantum dot nanoparticles to fabricate the memory devices[19, 20]. Like these, many groups have studied the combination of active materials to develop resistive memory devices.

The resistive memory characteristics such as unipolar, bipolar, WORM (write once read many) type are significant features of organic resistive random access memory (ReRAM) (see Figure 2).[21] The electrical performance of memory devices is assessed by I-V measurements which are conducted under a certain range of voltages. Within the range, the current is affected by the changes of resistance and show high and low resistive states. Polarizability of memory materials decides the type of memory, whether unipolar or bipolar. In case of unipolar, writing and erasing process happens at positive and negative voltage region independently; on the other hand, in case of bipolar, writing process happens during the positive voltage sweep and erasing process during the negative voltage. Not like these, WORM type has only one time writing and erasing process, so this type of memory is only able to read many times. These memory

characteristics were determined depending on the materials used.

Many mechanisms have been proposed to explain a switching phenomenon of organic memory devices (see Figure 3). The mainly suggested mechanisms of memory devices are filament, charge injection, and charge trapping theory.[22-24] The filament theory explains the switching phenomenon as a presence of metallic bridges between top and bottom electrodes. By applying voltage to devices, an oxidation and reduction of metal (top electrode) occurs inside the active layer by electrochemical process and forms the metallic bridges which transfer electrons from top to bottom electrodes. The flow of electrons through the metallic bridge leads to the change of resistance and operates the memory devices.

The second theory is charge injection theory. This theory originated from the energy barriers between active layer and electrodes. When the applied electric field exceeds the energy barrier, holes are injected into the HOMO level of electron donor material, and electrons are injected into the LUMO level of electron acceptor material. The charged HOMO and LUMO form a channel for charge carriers through charge-transfer interactions.

The last theory, the charge trapping theory (space charge limited current (SCLC) theory), is applied when the charge trapping materials such as metal nanoparticles, electron acceptors, and electron donors act as trap site in the insulating matrix. The traps capture the electrons and the insulating matrix protects from leakage. Due to the interruption of the flow of electrons, the resistance is changed. These can be simulated as an energy diagram and understood how the traps affect to the changes of resistance.

Here, we demonstrated a nonvolatile resistive organic memory device based on a PCBM (Phenyl-C61-butyric acid methyl ester) embedded in a phase separated

poly(styrene-*b*-methyl methacrylate) (PS-*b*-PMMA) diblock copolymer thin film. The diblock copolymers were used as an insulating layer between two terminal electrodes to contain the information storage materials. One of PS-*b*-PMMA diblock copolymers, PS_{10}-*b*-$PMMA_{130}$, developed spherical phase separation of the blocks according to the volume fraction of polystyrene block. We used this spherical phase of polystyrene to capture the PCBM. Hydrophobic PCBM is more likely to interact with polystyrene rather than poly(methyl methacrylate) having oxygen atoms. Due to the strong interaction between polystyrene and PCBM, the spherical phase of polystyrene can control the aggregation of PCBM. The aggregation of PCBM is critical to the memory devices because large scale aggregation can give rise to a conductive path. Through the path, the electrons can flow without the changes of resistance and interrupt the formation of memory effect. For this reason, controlling the aggregation is one of the factors that need to be considered for improved results.

The memory devices we demonstrated showed a bipolar characteristic and it remained continuously stable with reproducible behavior. We assume that these results were obtained due to the phase separation in the block copolymer. To compare the effect of phase separation of diblock copolymer, the devices were fabricated with homopolymer (polystyrene and poly(methyl methacrylate), respectively) which have the same molar weight with PS_{10}-*b*-$PMMA_{130}$, and PS_{52}-*b*-$PMMA_{8}$ which has opposite block ratio. As a result, these devices exhibited the deteriorative performance and shorter retention time than the block copolymer memory devices.

The mechanism we expect from our system is space charge limited current (SCLC) theory. PCBM works as the charge trapping material inside the PS-*b*-PMMA insulating layer and the spherical phase of PS-*b*-PMMA controls the aggregation of PCBM. The

mechanism was confirmed by fitting to appropriate conductance models on log-log scale.

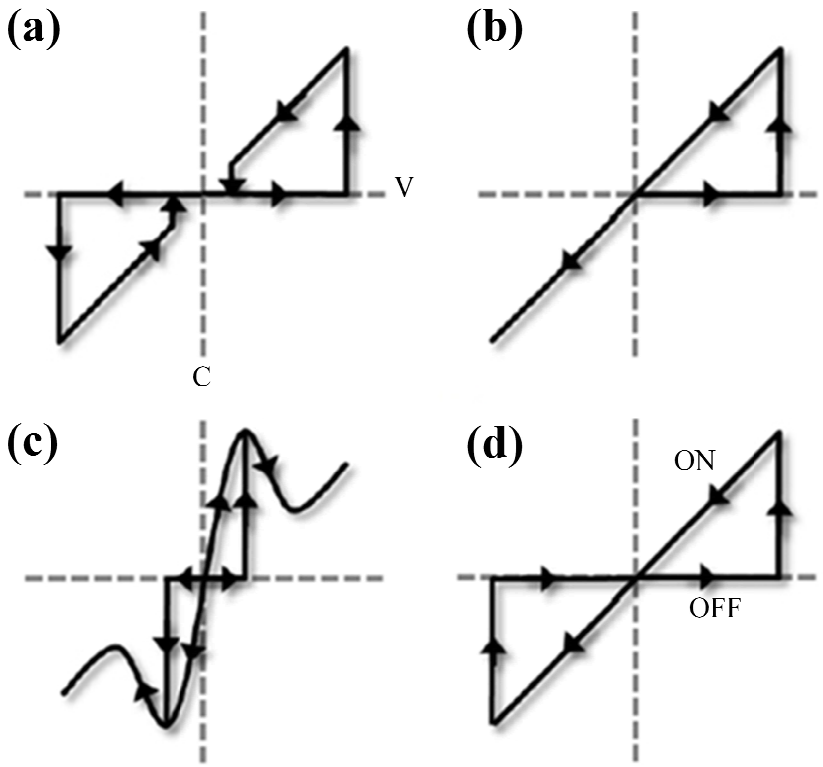

Figure 2. The I-V curves for the various types of memory devices: (a) Volatile switching, (b) Write-Once-Read-Many type switching (WORM), (c) Unipolar switching, and (d) Bipolar switching.[21]

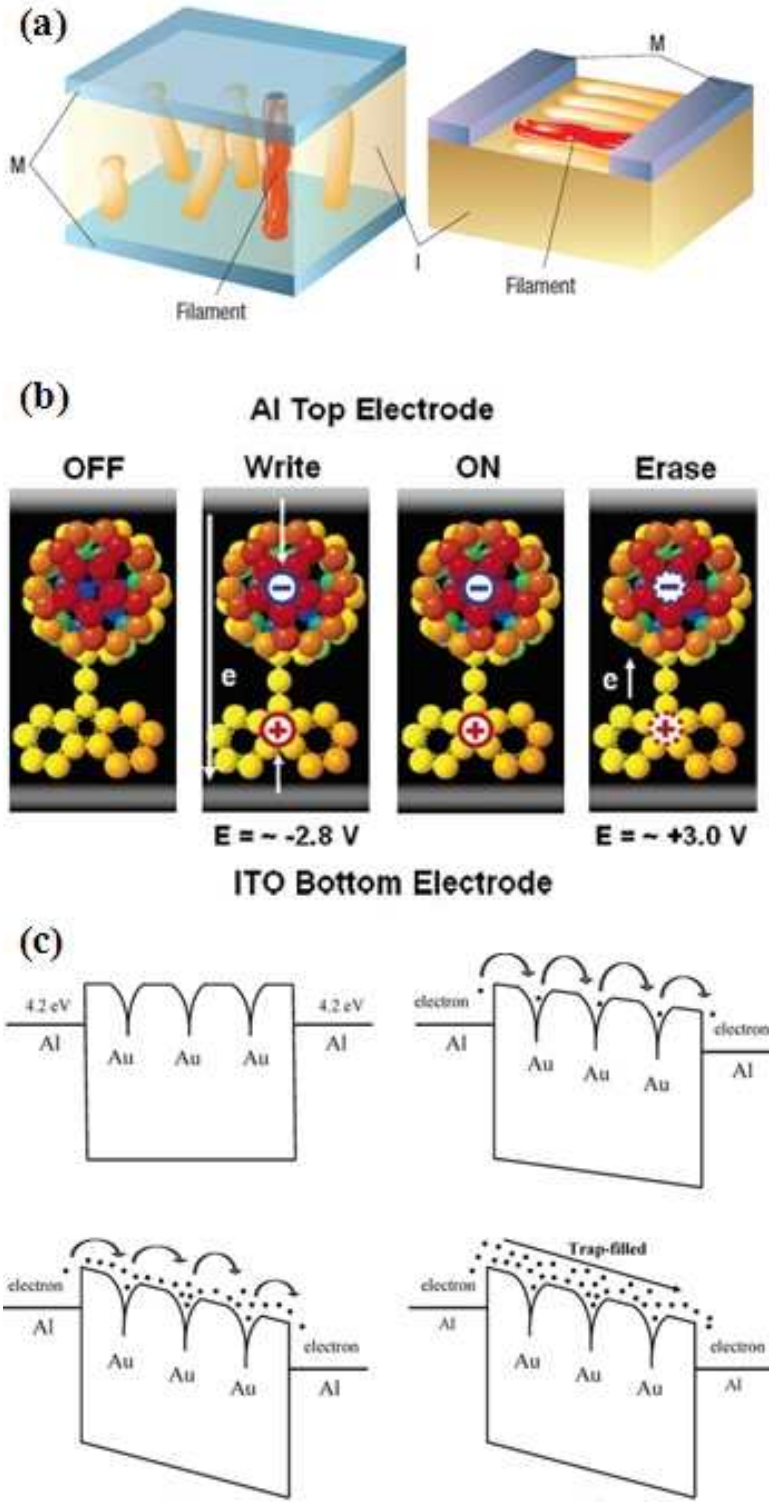

Figure 3. The schematic diagrams for the mechanism of ReRAM: (a) The filament theory, (b) The charge injection theory, (c) The Space Charge Limited Current (SCLC) theory.[22-24]

1. 3. Block Copolymer (BCP)

In block copolymers, the polymer chains consist of two (or more) monomeric species linked by covalent bonding. Because the block copolymer contains different polymer blocks, it has an inclination to self-assemble into a specific phase according to the properties of each block and their respective volume fraction. The phase separation takes place on the nanometer scale and these phases of block copolymer have been utilized as a template for obtaining periodic nanostructures.[25-27] The factors to determine the phase of block copolymer are the volume fraction of each blocks and the interblock segregation strength which is acquired from the Flory-Huggins parameter (χ) and degree of polymerization (N) (see Figure 4).[28-30] The Flory-Huggins parameter (χ) is related with a solubility parameter, therefore the solvent used to dissolve block copolymer should be determined carefully. The diagram shows that a block copolymer thin film can develop various kinds of internal structures such as spheres, cylinders, gyroid, and lamellar according to the polymer composition.

In this thesis, PS_{10}-*b*-$PMMA_{130}$ and PS_{52}-*b*-$PMMA_{8}$ were used to form the spherical structures and we confirmed that PS_{10}-*b*-$PMMA_{130}$ developed into the spherical structure by transmission electron microscopy (TEM) plan-view micrographs. In case of PS_{10}-*b*-$PMMA_{130,}$ polystyrene blocks are separated into spherical structures inside the poly(methyl methacrylate) matrix and the size of spheres is approximately 10nm.

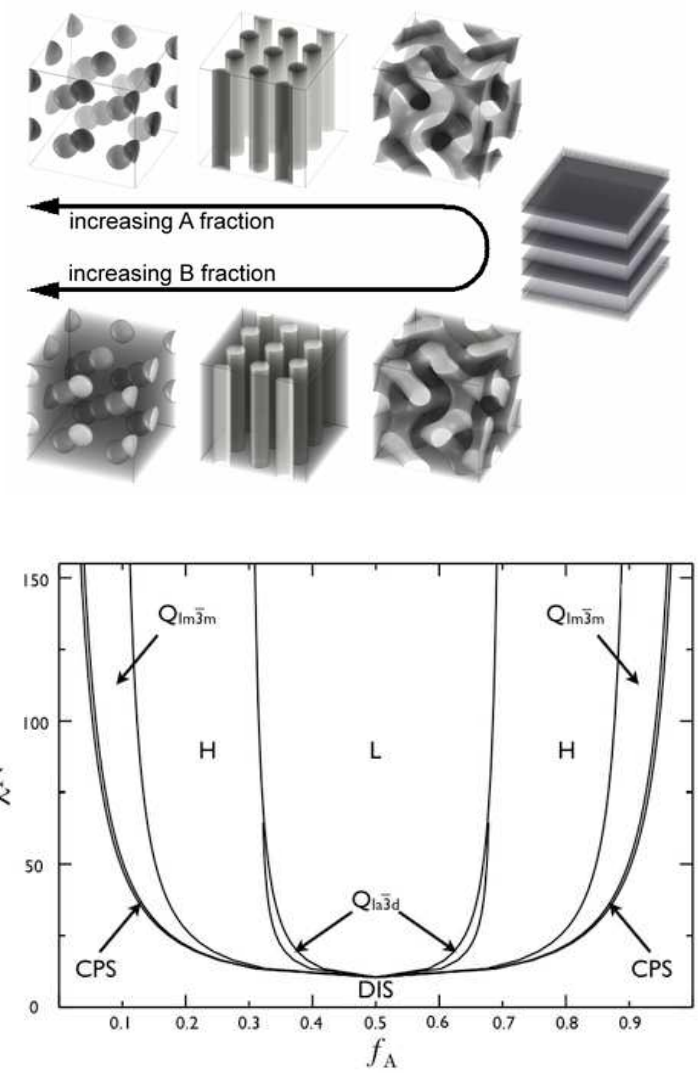

Figure 4. Diblock copolymer phase diagram (χN = degree of incompatibility, f_A = volume fraction of A block) as calculated using Mean-field Theory by Matsen and Bates with the various morphologies of block copolymer (L = lamellar, H = hexagonal cylinders, Q_{Ia3d} = bicontinuous cubic gyroid, Q_{Im3m} = BCC spheres, CPS = close-packed spheres, and DIS = disordered).[28-30]

2. Experimental Section

2. 1. Materials and Characterization

Poly(styrene-*b*-methyl methacrylate) (PS-*b*-PMMA) diblock copolymers: PS_{10}-*b*-$PMMA_{130}$ ($M_{n,PS}$ = 10 kg mol^{-1}, $M_{n,PMMA}$ = 130 kg mol^{-1}, PDI = 1.7) and PS_{52}-*b*-$PMMA_8$ ($M_{n,PS}$ = 52 kg mol^{-1}, $M_{n,PMMA}$ = 8 kg mol^{-1}, PDI = 1.06) were purchased from Polymer Source, Inc (Canada) and used as received. The weight fractions of PS for PS-*b*-PMMA (10-130) and (52-8) are calculated as 0.07 and 0.86, respectively, which yields spherical and inverse spherical morphology. [6,6]-phenyl-C61 butyric acid methyl ester (PCBM) was purchased from Nano-C Inc. Polystyrene (Mw=60,500) was purchased from Polymer Source, Inc and poly(methyl methacrylate) (Mw=100,000) was purchased from Polyscience, Inc. Toluene was purchased from Aldrich Inc. The chemical structures of materials are shown in Figure 5.

The I-V characteristics were measured using an Agilent 4155B semiconductor parameter analyzer at 300K under ambient condition. The thickness and morphology of the devices were characterized by optical microscopy (OM), confocal optical microscopy (confocal OM, Olympus LEXT OLS 3000), scanning electron microscopy (SEM, Hitachi S-4800), atomic force microscope (AFM, PSIA XE 100) and transmission electron microscopy (TEM, FEI Co. Technai F20) operated at 200 keV. The smallest objective aperture was used in order to obtain enough contrast in the bright field (BF) image and the images were recorded at large under-focus (-55.31um) condition which is much below Scherzer defocus, to visualize the separated morphology clearly. Even the size information can be significantly altered by changing the focus.

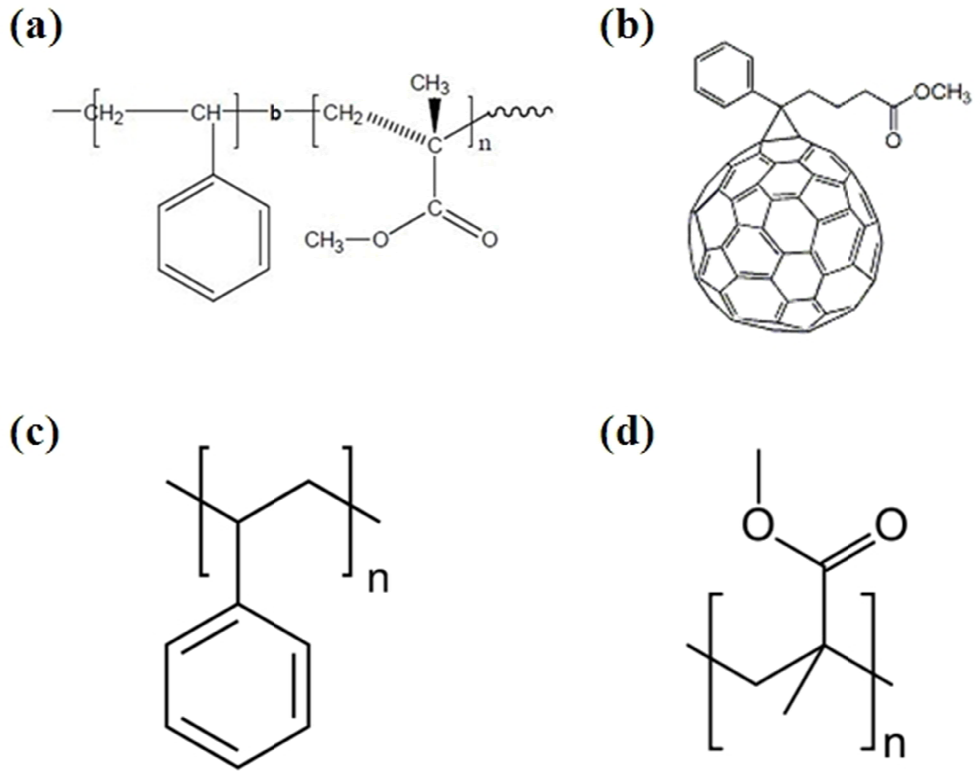

Figure 5. The chemical structures of materials: (a) Poly(styrene-*b*-methyl methacrylate) (PS-*b*-PMMA), (b) [6,6]-phenyl-C61 butyric acid methyl ester (PCBM), (c) Polystyrene, and (d) Poly(methyl methacrylate).

2. 2. Fabrication of Memory Devices

The diblock copolymer solution was prepared using 10mg PS-*b*-PMMA dissolved in 1mL toluene and stirred 12h under ambient conditions. The PCBM solution was separately prepared using 1mg PCBM (Nano-C Inc.) dissolved in 1mL toluene and treated in the same way as the diblock copolymer solution. After 12h various amount of PCBM solution was added to 1mL PS-*b*-PMMA solution in sequence and stirred overnight to obtain a homogeneous solution. As a reference, 5wt% polystyrene (Polyscience, Inc, Mw=60,500) and poly(methyl methacrylate) (Polyscience, Inc., Mw=100,000) solutions dissolved in toluene were prepared with the same conditions.

A 50~60-nm-thick PCBM:PS-*b*-PMMA nanocomposite layer was spin coated on the pre-washed indium-tin-oxide (ITO) glass at 500rpm for 30s, 3000rpm for 10s. After the nanocomposite thin film was formed, and remaining solvent was removed at 70℃ for 30min under N_2 atmosphere and the film was then additionally annealed at 140℃ for 12h in a vacuum oven to induce the phase separation of the block copolymer. When the devices were cooled down to room temperature, 150-nm-thick Al electrodes were thermally evaporated through a shadow mask (0.5 x 0.5 mm^2 in size) with a uniform deposition rate of 1$Å s^{-1}$. The composition of memory devices is aluminum top electrode, PCBM:PS-*b*-PMMA nanocomposite layer, and ITO bottom electrode (see Scheme 1).

2. 3. Preparation of TEM Samples

To prepare the sample for TEM plan view micrograph, the PCBM:PS-*b*-PMMA nanocomposite solution was spin coated on thin mica sheets at 500rpm for 30s, 3000rpm for 10s. After the nanocomposite thin film was formed, the standard annealing process was performed. The thin mica sheets were scratched by a blade to get a fine grid, and then the sheets were placed in DI water at an angle of 45 degrees. The water permeated the minute gap between the nanocomposite layer and the mica sheet and exfoliated the nanocomposite layer. The film floated on the water surface and can be collected by holey carbon TEM grids.

3. Results and Discussion

3.1. Characterization of PCBM:PS-*b*-PMMA Nanocomposite Thin Films

AFM (Atomic Force Microscopy) images of PS-*b*-PMMA diblock copolymer thin film containing 0.05wt% PCBM (relative to the weight of PS-*b*-PMMA) revealed a massive micro-sized hole and island structure (see Figure 6). This morphology of diblock copolymer thin films was mainly caused by the lattice mismatch. The lattice mismatch is determined by an incongruity between the equilibrium period (the period which the blocks form an uniform thin layer) and the film thickness.[31, 32] Consequentially, hole and island structures are formed when the film thickness is not perfectly matched with the equilibrium period of the diblock copolymer blocks. The block copolymer we used (PS_{10}-*b*-$PMMA_{130}$) has extremely short PS blocks and relatively long PMMA blocks; therefore, the morphology of film is strongly influenced by PMMA. The relatively large amount of PMMA tends to form a single PMMA thin film rather than surrounding PS blocks, so the islands which consist of PS spherical phase and PMMA matrix were formed onto the PMMA thin film. The diameter of holes was approximately 1μm and the depth of holes was 30~40nm.

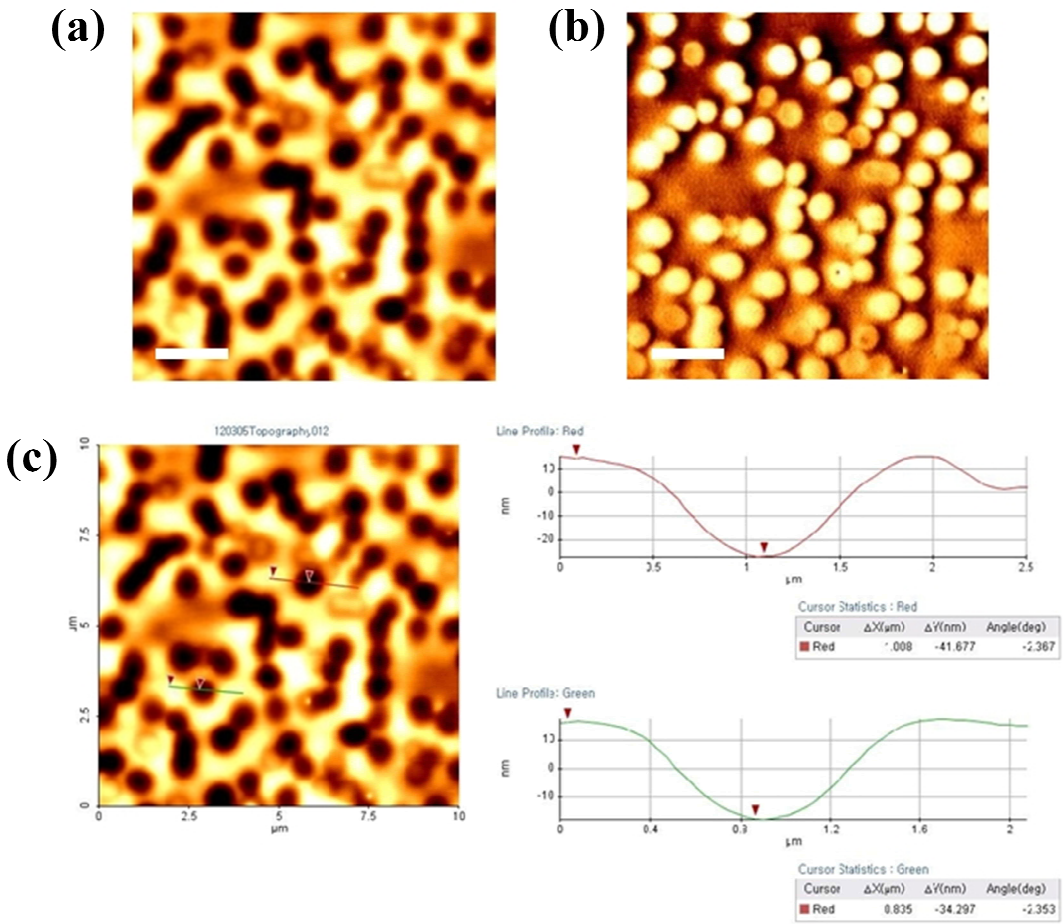

Figure 6. AFM images of the 0.05 wt% PCBM: 1wt % PS_{10}-*b*-$PMMA_{130}$ nanocomposite memory devices. (a) Height image. (b) Phase image. (c) Depth profile of the height image. The scale bars in Figs. 6(a) and 6(b) are 20um.

The TEM plan view micrographs revealed a spherical morphology of PS_{10}-*b*-$PMMA_{130}$ diblock copolymer thin films. This result supported that the phase of PS_{10}-*b*-$PMMA_{130}$ diblock copolymer were properly separated according to the PS block properties (the weight fraction = 0.07). The spherical phase of polystyrene was surrounded by poly(methyl methacrylate) matrix and the size of PS spheres was approximately10 nm (see Figure 7 (a)).

To confirm the influence of PCBM on the block copolymer's phase separation, 0wt%, 0.05wt%, 0.5wt%, 2.5wt%, 5wt%, and 25wt% PCBM were loaded to block copolymer solution and spin-coated onto the ITO glasses. Figure 7 shows that PS_{10}-*b*-$PMMA_{130}$ diblock copolymer thin films containing up to 0.5wt% PCBM has well-formed spherical structures. On the other hand, the structures of PS_{10}-*b*-$PMMA_{130}$ diblock copolymer with 5wt% and 25wt% PCBM were collapsed. This is because PCBM has a tendency to aggregate and develop needle-like crystals at the high annealing temperature, in case its concentration is too high. As a result, PCBM can be loaded into PS spheres up to a certain amount, but it deforms the film morphology above the threshold quantity.

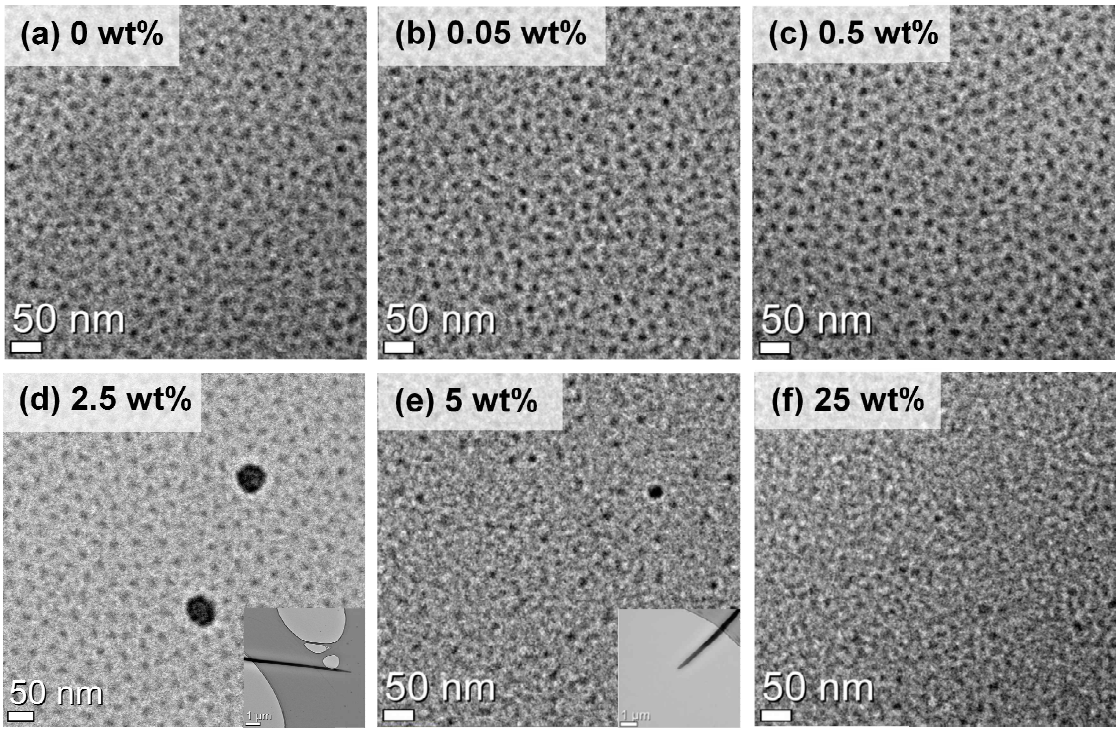

Figure 7. Plan view TEM images of PS_{10}-*b*-$PMMA_{130}$ nanocomposite thin film containing various wt% of PCBM. (a) 0wt%, (b) 0.05wt%, (c) 0.5wt%, (d) 2.5wt%, (e) 5wt% and (f) 25wt% of PCBM solution were added to PS_{10}-*b*-$PMMA_{130}$ diblock copolymer solution to form the thin films. The insets in Figs. 7(d) and 7(e) are the low magnification plan view TEM images that shows a needle-like PCBM crystal.

To verify the affinity between polystyrene and PCBM, an excess amount of PCBM solution was added to 5 wt% homopolymer solution (polystyrene and poly(methyl methacrylate)) and then spin-coated on ITO glasses. A thermal treatment (140℃, 12hrs) was applied analogously to the block copolymer thin films. The optical microscopy (OM) images of the films showed that only PCBM in the poly(methyl methacrylate) matrix separated as needle-like crystals whereas the PCBM at a PS sample was uniform (see Figure 8). It shows PCBM has better affinity with polystyrene.

In addition, Li et al confirmed the interaction between PS-*b*-P3HT and PCBM by quantum density functional theory.[33] The configuration of materials was simulated by computer and clearly shows that PCBM exists inside PS block (see Figure 9). The result shows the strong interaction between PS block and PCBM molecules and the possibility that PCBM can be accumulated within the PS blocks. It supports our assumption that PCBM was more likely to interact with polystyrene rather than poly(methyl methacrylate).

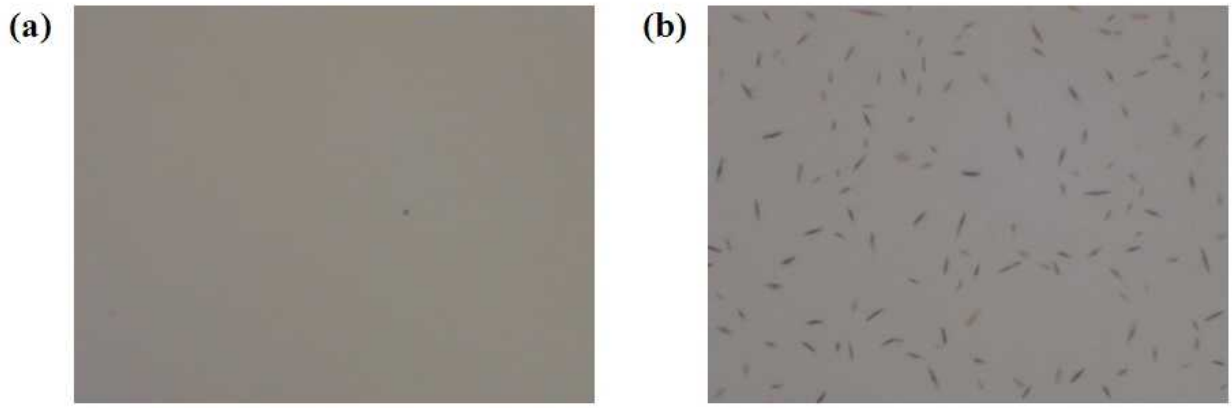

Figure 8. OM images of homopolymer and PCBM blended thin films. (a) 5wt% Polystyrene thin film containing 50wt% PCBM. (b) 5wt% Poly(methyl methacrylate) thin film containing 50wt% PCBM.

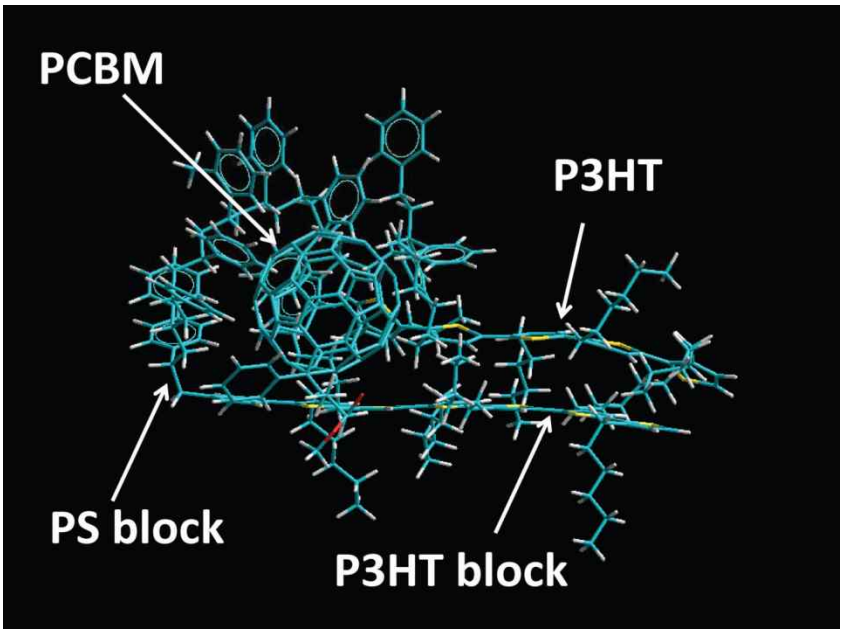

Figure 9. The molecular snapshot obtained from a 100 picosecond molecular dynamics simulation of an oligomeric blend of P3HT/PCBM with a single copolymer chain of PS-*b*-P3HT.[33]

To investigate whether formation of metallic bridges between the two terminal electrodes occur, Transmission Electron Microscopy (TEM) Energy-dispersive X-ray spectroscopy (EDX) analysis was performed (see Figure 10). The data showed that there was no penetration of metal and only copper peaks from the copper TEM grid were observed even at the interface between the top electrode and PCBM: PS_{10}-*b*-$PMMA_{130}$ nanocomposite layer. This shows that the PCBM: PS_{10}-*b*-$PMMA_{130}$ nanocomposite memory devices were operated by information storage material (PCBM) surrounding PS_{10}-*b*-$PMMA_{130}$ block copolymer. PCBM, a well-known electron acceptor, worked as the charge trapping material; therefore we assumed the mechanism of memory devices would be the space charge limited current (SCLC) theory instead of filament theory. The full details about SCLC theory will be discussed later.

The thickness of PCBM: PS_{10}-*b*-$PMMA_{130}$ nanocomposite layer was measured by transmission electron microscopy (TEM) cross-sectional micrograph, and yield in a value of approximately 50nm (see Figure 11). This thickness of the active layer is suitable for fabricating the ReRAM devices.

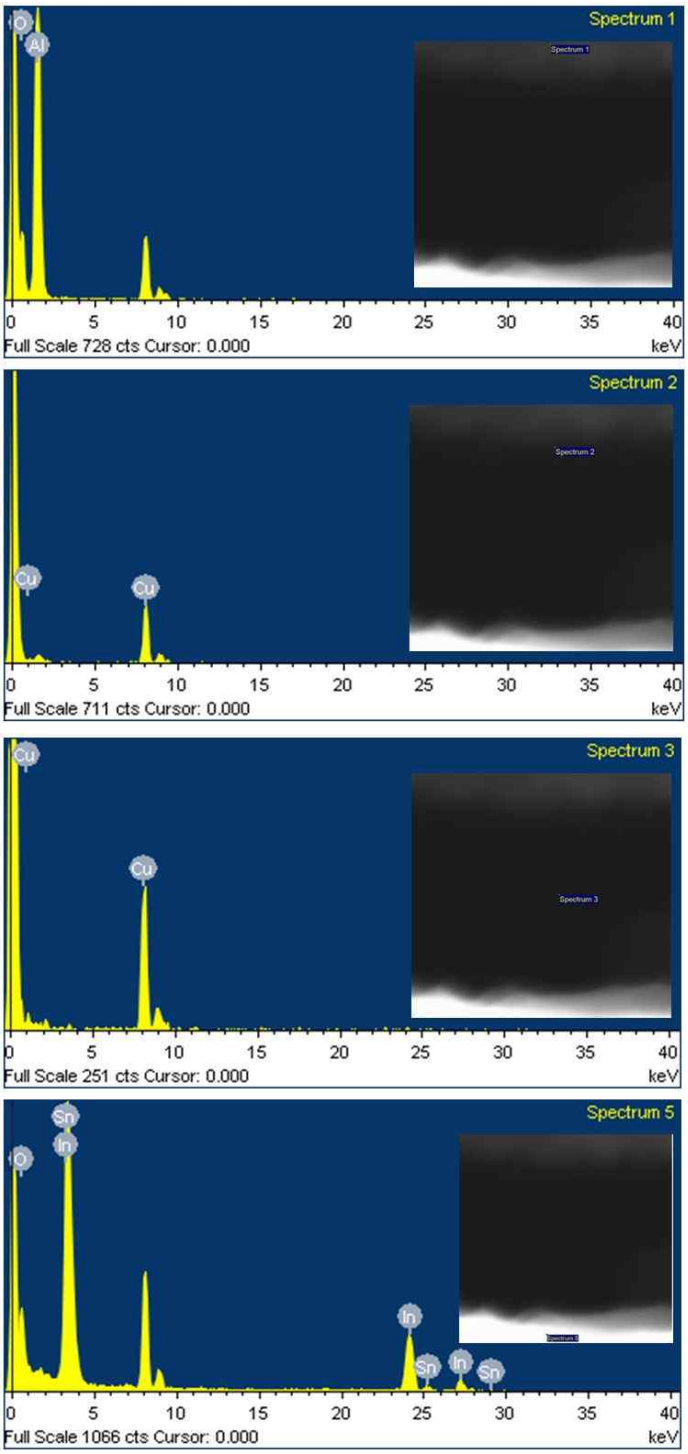

Figure 10. TEM EDX data of the Al/PCBM:PS_{10}-*b*-$PMMA_{130}$/ITO glass device.

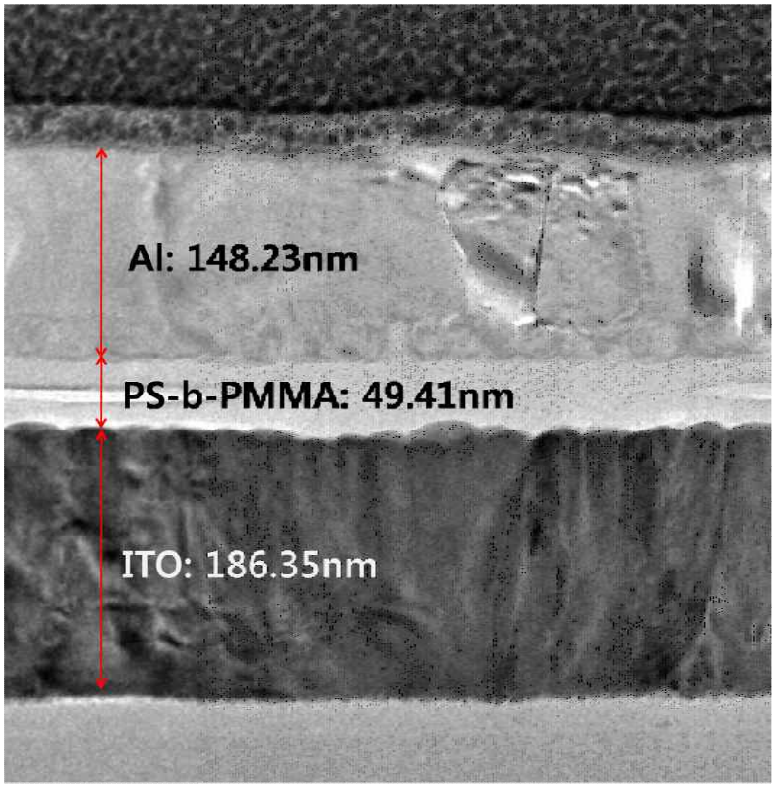

Figure 11. TEM cross-sectional micrograph of Al/PCBM:PS_{10}-*b*-$PMMA_{130}$/ITO glass device with the thickness of each layers.

3.2. Electrical Characteristics of PCBM:PS-*b*-PMMA Nanocomposite Memory Devices

The memory performance was investigated by current-voltage (I–V) measurements. Figure 12 (a) shows the I-V curves for the Al/PS_{10}-*b*-$PMMA_{130}$: PCBM/ITO glass device obtained by sweeping the applied voltage from 2 to -2V. Within the voltage sweep region, two distinct conductive states were shown clearly. The high- and low-conductivity states indicate ON state and OFF state, respectively. Figure 12 (a) shows the device exhibited low conductivity state (OFF state) between 2 and -2 V (region 1 and 2) which indicated the electrons started to trap in PCBM and kept the resistance high until all traps were filled. When the applied voltage was approximately -1.5V (end of region 2), the current abruptly increased and the device was switched to the high conductivity state (region 3) as the electrons could flow since all traps had been filled. The high conductivity state (ON state) of the device was maintained until the device was switched back to initial low conductivity state (OFF state) by reverse bias. When the voltage was swept from 0 to 2V (region 4), the device state returned to low conductivity state (OFF state) around 1.3V.

The I-V curve results indicate that the memory devices possess bistability and write and erase information stably at the low operating voltage. The maximum ON/OFF current ratio of the Al/PS_{10}-*b*-$PMMA_{130}$: PCBM/ITO glass device was approximately $\sim 10^2$ at reading voltages of -0.8V. To verify the reproducibility of devices, retention and endurance tests of Al/PS_{10}-*b*-$PMMA_{130}$: PCBM/ITO glass devices were also conducted. At a reading voltage of -0.8V, the distinct ON and OFF state were observed and maintained over 3×10^3 seconds (Figure 12 (b)) and 45 times repeated cycling (Figure 12

(c)). The retention and endurance test confirmed that the device worked stably as a nonvolatile resistive memory device.

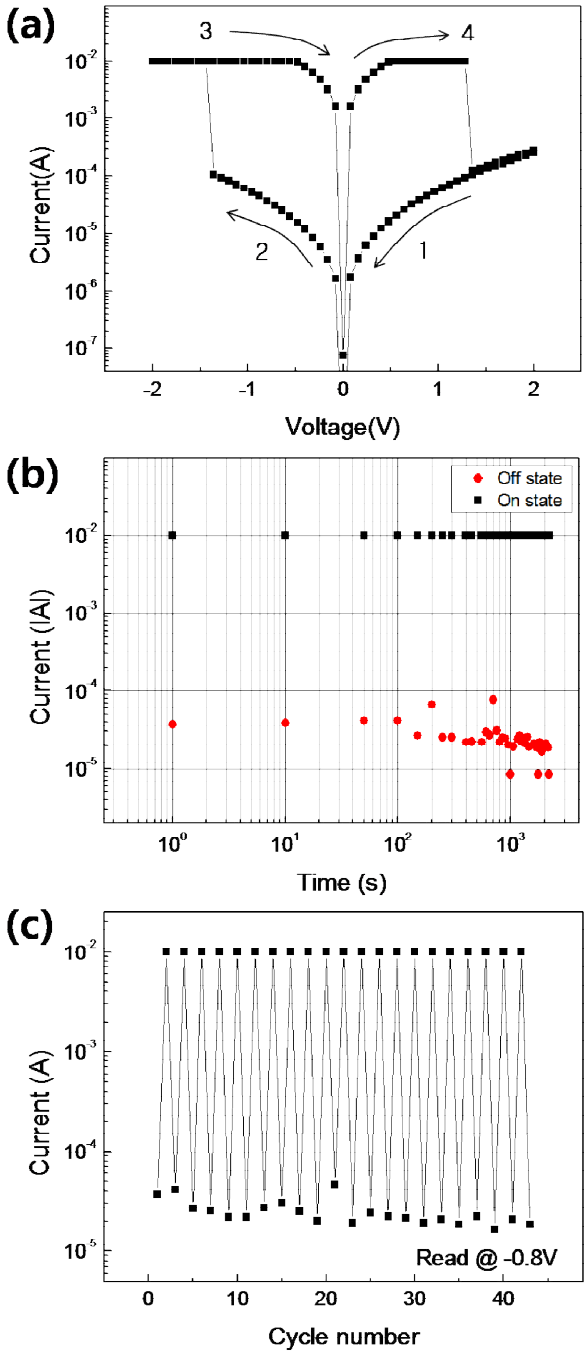

Figure 12. (a) The current-voltage curve of the Al/ PS_{10}-*b*-$PMMA_{130}$: PCBM (0.05wt%) /ITO glass device. The voltage swept from 2 to -2 V. (b) Retention test and (c) Endurance test of the device.

Different concentration of PCBM (0.5wt% and 2.5wt%) were added to the PS_{10}-*b*-$PMMA_{130}$ block copolymer solution to exam the correlation between the amount of information storage materials and the size of memory window (ON/OFF ratio). Figure 13 shows the electrical characteristics of 0.5wt% PCBM: PS_{10}-*b*-$PMMA_{130}$ and 2.5wt% PCBM: PS_{10}-*b*-$PMMA_{130}$ memory devices. The I-V curves reveal that the memory window is gradually decreased by adding more PCBM and the memory device finally acquires a constant resistance state. These results are caused by the collapse of the block copolymer's spherical phase. The TEM images which were already mentioned before shows the collapse of structure with increase of PCBM (see Figure 7). The spherical phase of block copolymer was retained up to the certain amount and collapsed suddenly. The PCBM aggregated into needle-like crystal after the structure was collapsed and the crystal acts as a conductive path; therefore, the memory window was shrunk. As a result, the amount of PCBM (below 2.5wt%) should be kept to keep the desired block copolymer structure and produce improved electrical performance of memory devices.

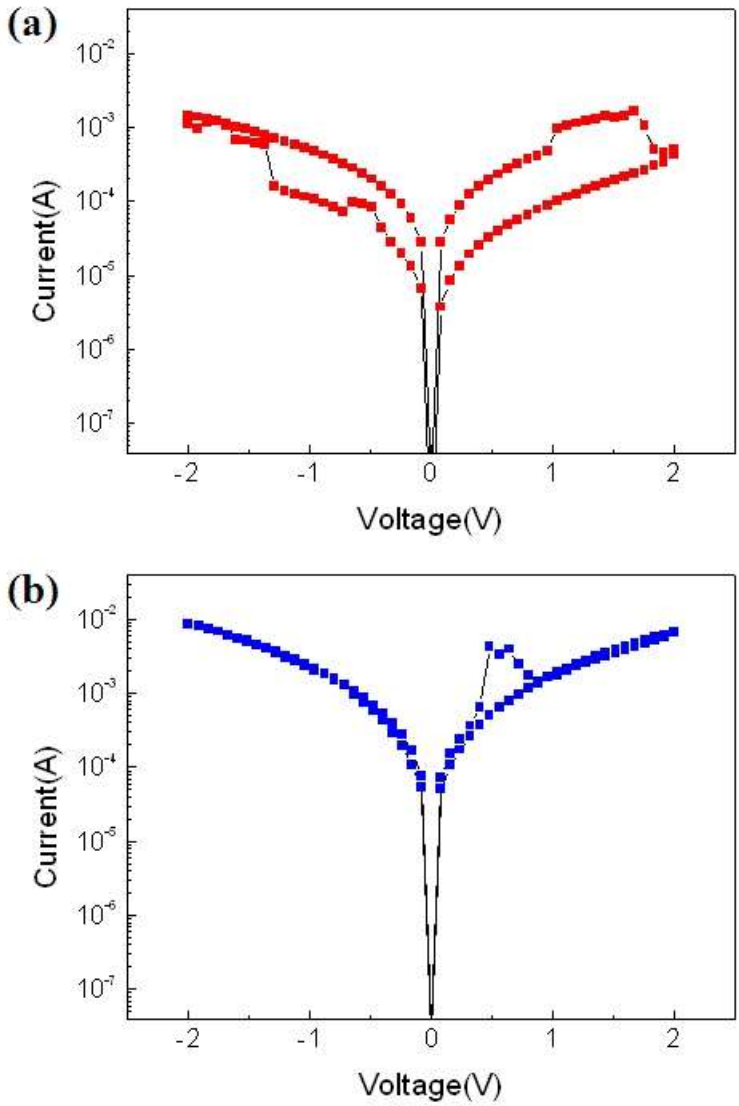

Figure 13. The I-V curves of the Al/PCBM:PS_{10}-*b*-$PMMA_{130}$/ITO glass device with different amount of PCBM: (a) 1wt% PS_{10}-*b*-$PMMA_{130}$ containing 0.5wt% PCBM and (b) 1wt% PS_{10}-*b*-$PMMA_{130}$ containing 2.5wt% PCBM.

As a further application, the PS_{10}-*b*-$PMMA_{130}$: PCBM nanocomposite memory devices were fabricated on a flexible ITO PET film. The reliable memory characteristics such as a sufficiently large ON/OFF ratio and clear SET/RESET process were obtained also in this case (see Figure 14). The ON/OFF ratio was similar to that of the block copolymer memory devices fabricated on the glasses. The greatest advantage was that the performance of memory devices was maintained without a remarkable degradation before and after bending. Even though the set voltage was shifted after bending, the response of current during the voltage sweep was similar. The I-V curves show bistability and possibility that the flexible memory devices can be realized. We expect the fully transparent and flexible memory devices will be produced by applying new types of electrodes and substrates.

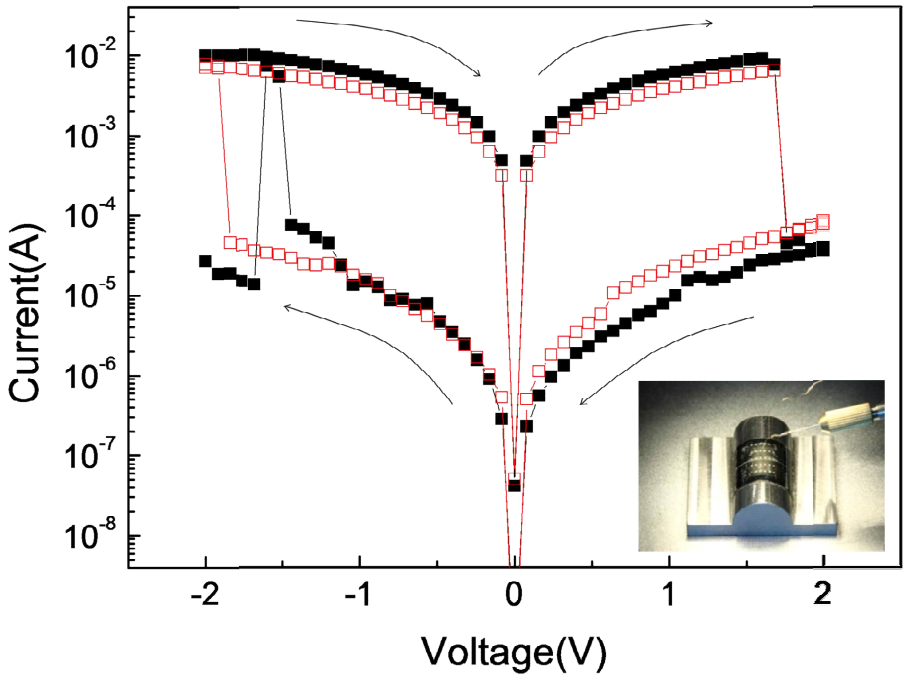

Figure 14. The I-V curve of Al/PS_{10}-*b*-$PMMA_{130}$ containing 0.1wt% of PCBM/ITO PET film device: (a) before and (b) after bending. The inset photograph represents the device in a bending holder with a radius curvature of 10mm.

As reference, the Al/PS_{52}-*b*-$PMMA_8$: PCBM/ITO glass memory devices were fabricated on the assumption that polystyrene has a preferable affinity with PCBM. We assumed the aggregation of PCBM cannot be controlled by the phase of PS_{52}-*b*-$PMMA_8$ because polystyrene becomes a matrix instead of a separated phase. The confocal OM images show the morphology of various films (see Figure 15). Depending on the composition of materials, the condition of films was different. Generally, the films had irregular phases, while the 1wt% PS_{10}-*b*-$PMMA_{130}$ containing 0.1wt% PCBM film which showed the best performance had the clear spherical shape.

The I-V measurement was conducted to confirm the electrical characteristics of PS_{52}-*b*-$PMMA_8$: PCBM memory devices (see Figure 16). There were no significant differences by loading various amount of PCBM because PCBM could not be confined into a fixed space. PCBM embedded in PS_{52}-*b*-$PMMA_8$ lead to almost the same behavior for PCBM as embedded in polystyrene thin film; therefore, there was no enhancement of performance. The ON/OFF ratio of PS_{52}-*b*-$PMMA_8$: PCBM memory devices were one hundred times smaller than PS_{10}-*b*-$PMMA_{130}$: PCBM nanocomposite memory devices and the reset process did not occur properly.

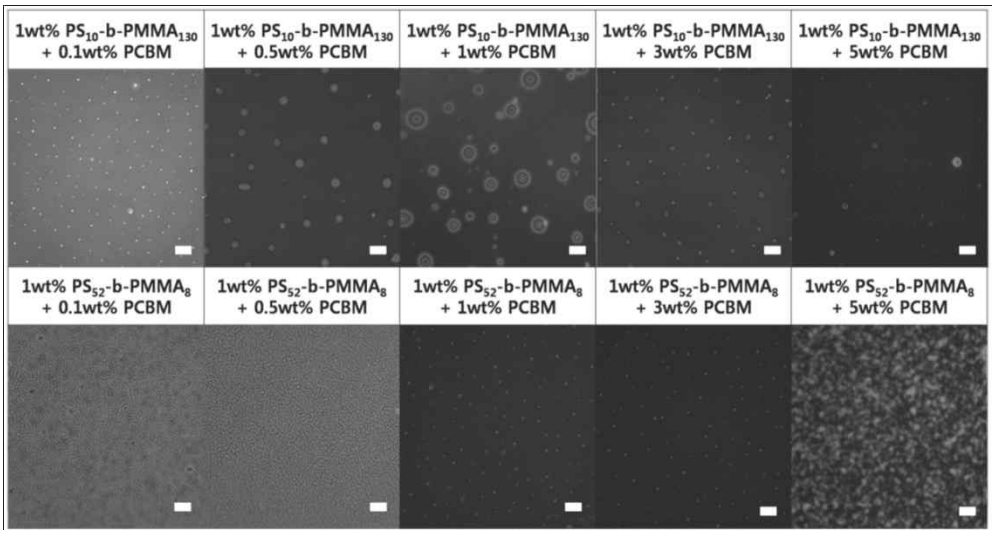

Figure 15. The confocal OM images of 1wt% PS_{10}-*b*-$PMMA_{130}$ and 1wt% PS_{52}-*b*-$PMMA_8$ block copolymer thin films containing various amount of PCBM. The scale bars are 5um.

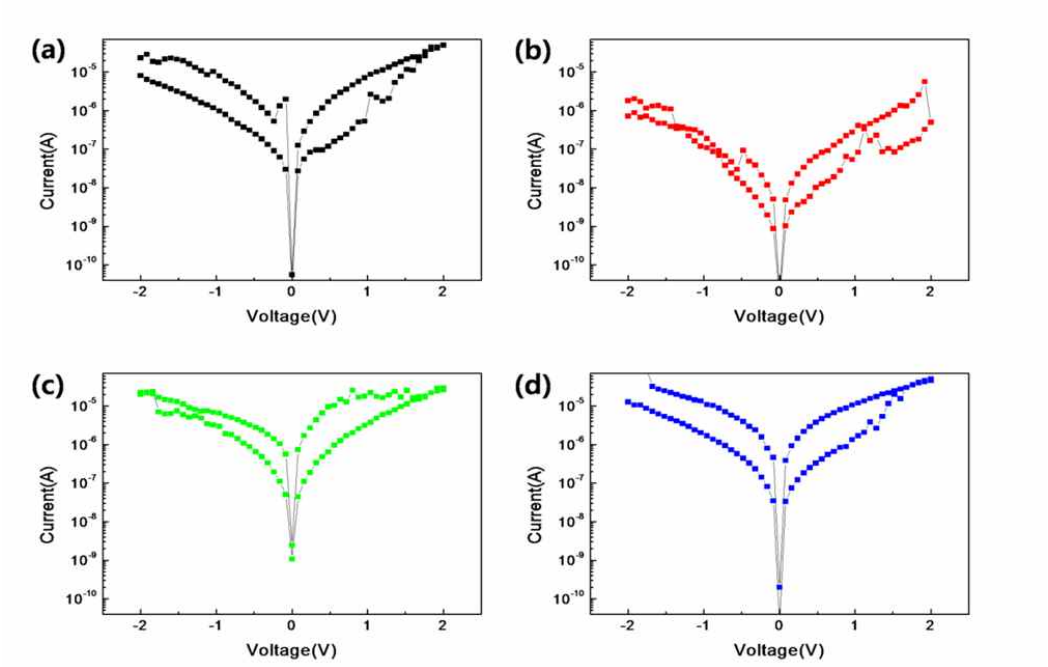

Figure 16. The I-V curves of Al/1wt% PS_{52}-*b*-$PMMA_8$ containing various wt% of PCBM/ITO glass devices. (a) 0.05wt% PCBM. (b) 0.5wt% PCBM. (c) 1.5wt% PCBM. (d) 2.5wt% PCBM.

To verify the advantage of the block copolymer, the I-V measurement of homopolymer: PCBM was also carried out. Figure 17 (a) and (b) show the I-V curve and retention of polystyrene and poly(methyl methacrylate), respectively. As a result, the performance of homopolymer: PCBM memory devices were unstable and irreproducible because they did not possess the capturing site inside the film. The ON/OFF ratio was much smaller than the block copolymer memory devices and the retention was also short, just as in the Al/PS_{52}-*b*-$PMMA_8$: PCBM/ITO glass memory devices. This result supports our assumption that the separated phase of block copolymer improved the electrical performance and facilitates the stable operation of memory devices.

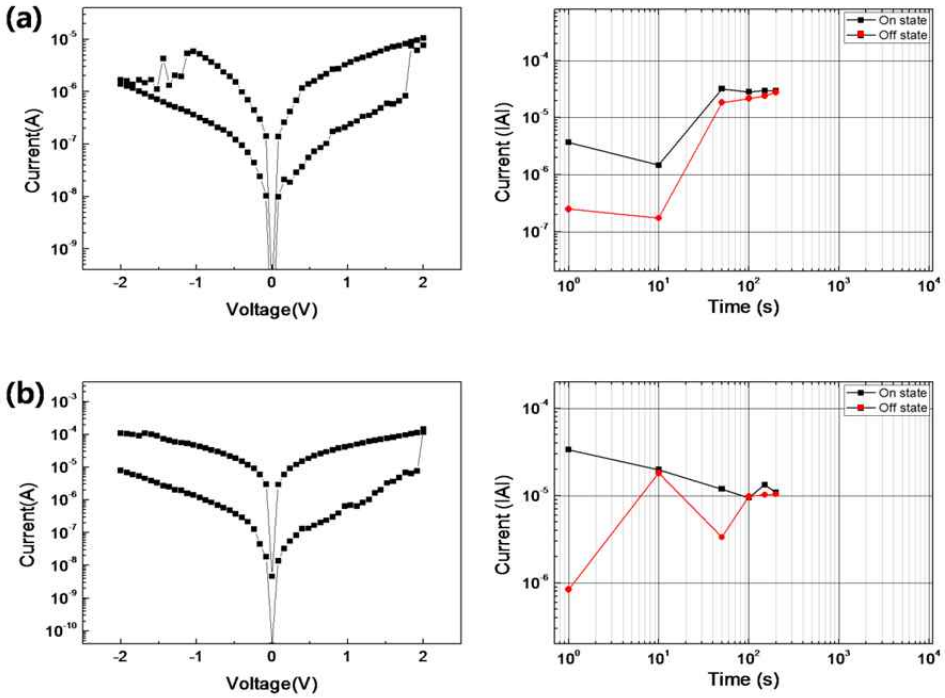

Figure 17. The I-V curves of the memory devices (left) and retention tests (right) (a) the device with the configuration of Al/PS containing 0.05wt% PCBM/ITO glass, (b) the device with the configuration of Al/PMMA containing 0.05wt% PCBM/ITO glass.

We assume that all block copolymer: PCBM memory devices follow the SCLC (Space Charge Limited Current) theory as the working mechanism. The mechanism was verified by fitting the I-V curves to log-log scale (see Figure 18). Many researchers have applied the SCLC theory as their mechanism.[34, 35] At the beginning stage, the electrons are injected by thermal energy from the aluminum top electrode to the active layer and start to trap inside PCBM, spreading out all over the active layer. The current followed the relationship; $I \propto V^2$ when the electrons were trapped in PCBM and then sharply increased at the threshold voltage (turn-on voltage) because the electrons have filled up all of the trap sites. The electron now flow following an ohmic process ($I \propto V$). The log scale I-V curve for the memory devices based on the phase separated block copolymer containing PCBM shows this behavior, confirming that the devices follow SCLC theory.

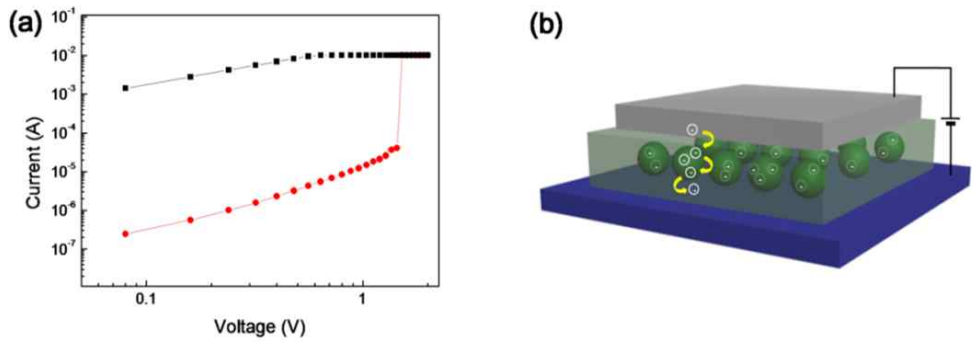

Figure 18. (a) A log-log plot of the current as a function of the voltage for Al/ PS_{10}-*b*-$PMMA_{130}$: PCBM (0.05wt%) /ITO glass device during the OFF state and ON state. (b) A hypothetical diagram for switching mechanism.

4. Conclusion

In conclusion, the nonvolatile organic memory devices based on the PCBM embedded in a phase separated PS-b-PMMA diblock copolymer thin films were demonstrated. The PS-b-PMMA diblock copolymer thin films were separated into the spherical structure according to the volume fraction of polystyrene block, 0.07. The 10nm sized polystyrene spheres captured PCBM inside and controlled the aggregation. Preventing the aggregation of PCBM improved the electrical performance of memory devices because the flow of electrons was well-controlled by the separated phase without the formation of conductive path. The maximum ON/OFF current ratio of the Al/PS_{10}-b-$PMMA_{130}$: PCBM/ITO glass device was approximately ~10^2 at reading voltages of -0.8V and the performance kept continuously over $3x10^3$ seconds. The flexible memory devices also showed the stable bipolar characteristic without changes before and after bending. On the other hand, the memory devices consisting of homopolymer and PCBM were unstable and irreproducible. From the results, we conclude that the well-separated spherical phase of block copolymer played a major role in improving the electrical performance of memory devices. The present study shows the improved performance of memory devices by using the block copolymer, and we believe our system can be applied to the large-area production such as the roll-to-roll process in the future.

Reference

1. Lee, M. H.; Yun, D. Y.; Park, H. M.; Kim, T. W. *Applied Physics Letters* **2011,** 99, (18).

2. Ji, Y.; Lee, S.; Cho, B.; Song, S.; Lee, T. *Acs Nano* **2011,** 5, (7), 5995-6000.

3. Kim, S. J.; Lee, J. S. *Nano Letters* **2010,** 10, (8), 2884-2890.

4. Kuang, Y. B.; Huang, R.; Tang, Y.; Ding, W.; Zhang, L. J.; Wang, Y. Y. *Ieee Electron Device Letters* **2010,** 31, (7), 758-760.

5. Lian, K.; Li, R.; Wang, H.; Zhang, J.; Gamota, D. *Materials Science and Engineering B-Advanced Functional Solid-State Materials* **2010,** 167, (1), 12-16.

6. Whitesides, G. M. *Abstracts of Papers of the American Chemical Society* **1996,** 212, 31-Inor.

7. Xia, Y. N.; Whitesides, G. M. *Angewandte Chemie-International Edition* **1998,** 37, (5), 551-575.

8. Di Ventra, M.; Pershin, Y. V. *Materials Today* **2011,** 14, (12), 584-591.

9. Fontana, R. E.; Hetzler, S. R.; Decad, G. *Ieee Transactions on Magnetics* **2012,** 48, (5), 1692-1696.

10. Yun, J. G.; Lee, J. D.; Park, B. G. *Solid-State Electronics* **2011,** 55, (1), 37-43.

11. Cho, S.; Shim, W. B.; Park, I. H.; Kim, Y.; Park, B. G. *Journal of the Korean Physical Society* **2010,** 56, (1), 137-141.

12. Cho, B.; Kim, T. W.; Song, S.; Ji, Y.; Jo, M.; Hwang, H.; Jung, G. Y.; Lee, T. *Advanced Materials* **2010,** 22, (11), 1228-+.

13. Baral, J. K.; Majumdar, H. S.; Laiho, A.; Jiang, H.; Kauppinen, E. I.; Ras, R. H. A.; Ruokolainen, J.; Ikkala, O.; Osterbacka, R. *Nanotechnology* **2008,** 19, (3).

14. Lee, M. H.; Jung, J. H.; Shim, J. H.; Kim, T. W. *Organic Electronics* **2011,** 12,

(8), 1341-1345.

15. Ji, Y.; Cho, B.; Song, S.; Kim, T. W.; Choe, M.; Kahng, Y. H.; Lee, T. *Advanced Materials* **2010,** 22, (28), 3071-3075.

16. Hsu, J. C.; Liu, C. L.; Chen, W. C.; Sugiyama, K.; Hirao, A. *Macromolecular Rapid Communications* **2011,** 32, (6), 528-533.

17. Chen, J. C.; Liu, C. L.; Sun, Y. S.; Tung, S. H.; Chen, W. C. *Soft Matter* **2012,** 8, (2), 526-535.

18. Yu, A. D.; Liu, C. L.; Chen, W. C. *Chemical Communications* **2012,** 48, (3), 383-385.

19. Kim, W. T.; Jung, J. H.; Kim, T. W.; Son, D. I. *Applied Physics Letters* **2010,** 96, (25).

20. Shim, J. H.; Jung, J. H.; Lee, M. H.; Kim, T. W.; Son, D. I.; Han, A. N.; Kim, S. W. *Organic Electronics* **2011,** 12, (9), 1566-1570.

21. Park, J.; Moon, W. *Microsystem Technologies-Micro-and Nanosystems-Information Storage and Processing Systems* **2003,** 9, (8), 511-519.

22. Waser, R.; Aono, M. *Nature Materials* **2007,** 6, (11), 833-840.

23. Lin, H. T.; Pei, Z.; Chan, Y. J. *Ieee Electron Device Letters* **2007,** 28, (7), 569-571.

24. Ling, Q. D.; Lim, S. L.; Song, Y.; Zhu, C. X.; Chan, D. S. H.; Kang, E. T.; Neoh, K. G. *Langmuir* **2007,** 23, (1), 312-319.

25. Hsueh, H. Y.; Huang, Y. C.; Ho, R. M.; Lai, C. H.; Makida, T.; Hasegawa, H. *Advanced Materials* **2011,** 23, (27), 3041-+.

26. Deshmukh, R. D.; Buxton, G. A.; Clarke, N.; Composto, R. J. *Macromolecules* **2007,** 40, (17), 6316-6324.

27. Jung, Y. S.; Ross, C. A. *Small* **2009,** 5, (14), 1654-1659.

28. Leibler, L. *Macromolecules* **1980,** 13, (6), 1602-1617.

29. Kielhorn, L.; Muthukumar, M. *Journal of Chemical Physics* **1999,** 110, (8), 4079-4089.

30. Matsen, M. W.; Bates, F. S. *Macromolecules* **1996,** 29, (4), 1091-1098.

31. Kim, Y. S.; Suh, K. Y.; Lee, H. H. *Physical Review E* **1997,** 56, (4), 4887-4889.

32. Lee, S. H.; Kang, H.; Cho, J.; Kim, Y. S.; Char, K. *Macromolecules* **2001,** 34, (24), 8405-8408.

33. Sun, Z. Z.; Xiao, K.; Keum, J. K.; Yu, X.; Hong, K. L.; Browning, J.; Ivanov, I. N.; Chen, J. H.; Alonzo, J.; Li, D. W.; Sumpter, B. G.; Payzant, E. A.; Rouleau, C. M.; Geohegan, D. B. *Advanced Materials* **2011,** 23, (46), 5529-+.

34. Baek, H.; Lee, C.; Park, J.; Kim, Y.; Koo, B.; Shin, H.; Wang, D. Y.; Cho, J. *Journal of Materials Chemistry* **2012,** 22, (11), 4645-4651.

35. Son, D. I.; Park, D. H.; Bin Kim, J.; Choi, J. W.; Kim, T. W.; Angadi, B.; Yi, Y.; Choi, W. K. *Journal of Physical Chemistry C* **2011,** 115, (5), 2341-2348.

요 약 (국문 초록)

상 분리가 일어난 poly(styrene-*b*-methyl methacrylate) (PS-*b*-PMMA) 블록 공중합체 박막에 Fullerene 계열의 탄소 물질인 PCBM 을 가두어 비 휘발성의 저항 변환성 메모리를 제작하였다. 이 실험에서 사용된 PS-*b*-PMMA 블록 공중합체는 두 고분자 블록의 성질에 따라 구형의 상으로 자기 조립하였다. PCBM 분자들이 구형의 상을 가지는 PS 나노 도메인 안에 선택적으로 격리됨으로써 응집 없이 잘 분산 시킬 수 있었고, PCBM 의 응집을 조절함으로써 더 향상된 성능을 가지는 메모리 소자를 제작할 수 있었다. PS-*b*-PMMA 블록 공중합체와 PCBM 의 나노 혼합체로 만들어진 메모리 소자는 bipolar 스위칭 현상을 보였으며 저 전압에서도 안정적으로 재생산성 있게 그 현상을 유지하였다. 이러한 결과는 불안정한 set/reset 현상과 짧은 성능 유지 시간을 가지는 단일 고분자:PCBM 혼합체 메모리 소자와 극명한 차이를 보여준다. 더 나아가 응용 방안으로서, PS-*b*-PMMA/PCBM 나노 구조를 이용하여 구부림 전, 후에 성능 감소가 없는 유연한 메모리 소자를 제작하였다. 간단한 용액 공정을 통해서 고성능을 가지고 저 전압 구동이 가능한 비 휘발성 저항 변환성 메모리를 추가 공정 없이 성공적으로 얻을 수 있었다.

주요어 : 블록 공중합체, PCBM, 저항 변환성 메모리, 비 휘발성 메모리, 유연한 소자

학 번 : 2010-23945